Synthesis and Characterization of Carboxylate−FeOOH Nanoparticles (Ferroxanes) and Ferroxane-Derived Ceramics

Jérôme Rose,*,† Maria M. Cortalezzi-Fidalgo,‡ Stephane Moustier,† Cyrille Magnetto,† Christopher D. Jones,§ Andrew R. Barron,§ Mark R. Wiesner,‡ and Jean-Yves Bottero†

CEREGE Equipe physico-chimie des interfaces, UMR 6635 CNRS/Université Aix-Marseille III, Europole Méditerranéen de l'Arbois, BP80, 13545 Aix en Provence Cedex 4, France, and Departments of Environmental Science and Engineering, Chemical Engineering, Chemistry, and Mechanical Engineering and Materials Science, Rice University, 6100 Main Street, Houston, Texas 77005-1892

Received June 12, 2001. Revised Manuscript Received October 18, 2001

A new environmentally benign process for producing Fe-based ceramics of variable properties is presented. We have demonstrated that the reaction between lepidocrocite and acetic acid (=AA) in water results in the formation of carboxylate−FeOOH nanoparticles called ferroxane−AA analogous to aluminum-based alumoxanes. The structure of the ferroxane particles consists of an FeOOH core part with the structure of the lepidocrocite (γ-FeOOH), coated with AA. FTIR and EXAFS at the Fe K edge indicates that AA is chemically adsorbed onto the FeOOH core part. The size of these ferroxanes is 0.3 μm composed of nanodomains of 20−30 Å with a γ-FeOOH structure. Thermolysis of the ferroxane−AA yields Fe oxide ceramics. The specific surface area of 134 m^2/g does not increase from the initial mineral to the ferroxane while the pore size distribution becomes monodisperse and the diameter of the pore size decreases from 55 to 12 and 13 nm after the firing of the ferroxanes. Moreover, the ferroxane−AA has been successfully doped with metal to form a precursor for Fe mixed-metal oxides. Upon thermolysis the products evolve to homogeneous Fe−metal oxides. A low firing temperature for conversion to ceramic as well as the use of environmentally benign feedstock suggest that the process for creating ferroxane-derived ceramics should have minimal environmental impacts.

1. Introduction

Iron oxides are widely used in industry with applications including pigments for paints, materials introduced for medical procedures, building materials, chemical sorbents, and catalysts.[1,2] The toxicity of iron oxide and oxyhydroxides is negligible. Unfortunately, their synthesis generates numerous organic pollutants. Two common processes are used to produce various oxide ceramics. Powder processing, shape forming, and densification are typically used to produce bulk quantities of material. The shape-forming step is the most environmentally toxic stage because various binders, solvents (often chlorinated such as 1,1,1-trichloroethylene = TCE[3]), and other potentially toxic agents are added. A second process for the formation of ceramic films is the sol−gel process. It involves four different steps: dispersion, gelation, drying, and firing.[4] The crucial point in this four-stage process is the creation of a stable liquid dispersion, or *sol*, of the colloidal ceramic precursors. To achieve this goal, several solvents with appropriate additives are added to the initial solution. Environmentally harmful consequences arising from the sol−gel process may arise for the use of strong acids, plasticizers, binders, solvents, and *sec*-butanol formed during the reaction.

A more environmentally benign alternative to the sol−gel process has been reported in the case of Al−ceramic synthesis.[5] This process is based upon alumoxanes (species containing oxo (O^{2-}) bridges between Al atoms) prepared directly from a mineral named boehmite (γ-AlOOH).[6,7] This pathway that goes from a

* To whom correspondence should be addressed. E-mail: rose@cerege.fr.

† UMR 6635 CNRS/Université Aix-Marseille III.

‡ Department of Environmental Science and Engineering and Department of Chemical Engineering, Rice University.

§ Department of Chemistry and Department of Mechanical Engineering and Materials Science, Rice University.

(1) Shwertmann, U.; Cornell, R. M. *Iron Hydroxyde in the Laboratory*; VCH: New York, 1991.

(2) Shwertmann, U.; Cornell, R. M. *The Iron Oxides-Structure, Properties, Reactions, Occurrence and Uses*; VCH: New York, 1996.

(3) Sawyer, C.N.; McCaryr, P. L.; Perkin, G. F. *Chemistry for Environmental Engineering*; McGraw-Hill: New York, 1994.

(4) See, for example, Serna, J.; White, L.; Hem, S.L. Sol−Gel Science: The Physics and Chemistry of Sol−Gel Processing. *Sol. Sci.* **1977**, *41*, 1009. Brinker, C. J.; Sherer, G.W. *Sol−Gel Science: The Physics and Chemistry of Sol−Gel Processing*; Academic Press: San Diego, CA, 1990.

(5) Callender, R. L.; Harlan, C. J.; Shapiro, N. M.; Jones, C. D.; Callahan, D. L.; Wiesner, M. R.; MacQueen, D. B.; Cook, R.; Barron, A. R. *Chem. Mater.* **1997**, *9*, 2418.

(6) Apblett, A.W.; Warren, A.C.; Barron, A.R. *Chem. Mater.* **1997**, *4*, 161.

(7) Landry, C. C.; Davis, J. A.; Apblett, A. W.; Barron, A. R. *J. Mater. Chem.* **1997**, *3*, 597.

10.1021/cm010583r CCC: $22.00
Published on Web 02/18/2002

mineral to clusters or colloids is the reverse of the sol−gel process that starts from the Al or metal monomer in solution and evolves through polymerization of Al monomers to AlOOH particles. Carboxylate−alumoxane (=C−alumoxane) $[Al(O)_x(OH)_y(O_2R)_z]_n$ were synthesized by the reaction of boehmite with different carboxylic acids, leading to infinite stable products at ambient conditions in a solid as well as in solution. Alumoxane nanoparticles may deposit on a substrate and, upon thermolysis, these C−alumoxanes are converted to an alumina ceramic film. These C−alumoxanes may also be doped with transition metals or lanthanide as a route to ternary aluminum based ceramics.[8]

It is well accepted that FeOOH and Fe_2O_3 are more resistant to acidic, corrosive, and oxidant conditions than AlOOH and alumina.[2,9] Moreover, Fe minerals are found to be more reactive toward heavy metals than Al minerals.[10,11]

The objectives of the present study were (a) to prepare carboxylate−FeOOH = ferroxane, that is, a new Fe precursor for Fe−ceramics, in water, (b) to determine the structure of these ferroxanes, (c) to test their capacities to form Fe_2O_3 ceramics with desired textural properties, and (d) to dope ferroxanes with transition metals to obtain a ternary ceramic of interest for catalysis. The characterization methodologies are based on our previous work concerning the study of Fe salt hydrolysis and polymerization, FeOOH minerals precipitation,[12−15] and alumoxane-derived membranes synthesis.[16]

2. Experimental Section

2.1. Material. Two Fe oxyhydroxides α- and γ-FeOOH named goethite and lepidocrocite, respectively, were used to investigate the influence of the crystallography of the initial mineral on the structure and size of the resulting ferroxanes. Both FeOOH minerals were synthesized from $FeCl_2{\cdot}4H_2O$ acidic solution.

Synthesis A. $FeCl_2{\cdot}4H_2O$ powder (5.73 g) (Merck) was added to 500 mL of ultrapure (UP) water. The pH was adjusted to 7 with NaOH solution. The solution was oxidized with air. The pH of the solution was maintained at 7 by the addition of NaOH for 4 h at room temperature. This experiment leads to a mixture of α- and γ-FeOOH minerals (detailed further) referred to as **Goet**−**Lep**.

Synthesis B. $FeCl_2{\cdot}4H_2O$ solution (100 mL) was mixed with a NaOH solution. The ratio $R = [FeCl_2{\cdot}4H_2O]/[NaOH] = 0.6$ favors the formation of a pure lepidocrocite.[17] We used an $FeCl_2{\cdot}4\ H_2O$ solution at 0.06 mol/L with Fe. This sample composed of 100% of γ-FeOOH was referred to as **Lep**.

Ferroxane Formation. These two starting materials (**Goet**−**Lep** and **Lep**) were put in contact with acetic acid (AA) (Aldrich). Two grams of both materials and 2.572 mL = 4.28×10^{-2} mol of a 100% acetic acid solution were refluxed in water (50 mL) at 80 °C for 1 night. The [Fe]/[AA] ratio was 1.5. The solution was centrifuged at 20 000 rpm for 2 h and the volatiles were removed in a vacuum (10^{-2} Torr) at 90 °C. These products, called **ferroxane**−**AA**, were fired at 300 °C to obtain a ceramic.

Doped Ferroxane. The **ferroxane**−**AA** formed with the **Lep** initial sample was tested for doping with other elements. The first test was made with zirconium. The doped ferroxane was prepared by mixing a solution of 14 g/L of ferroxane and a Zr acetylacetone (=Zracac) solution ($[Zr] = 1.5 \times 10^{-2}$ mol L^{-1}). The reaction was stirred at 80 °C overnight.

2.2. Methods. The XRD analyses were carried out with a Philips PW 3710 X-ray diffractometer using Co Kα radiation at 40 kV and 40 mA.

AFM measurements were made on a Nanoscope IIIa scanning probe microscopic controller (Digital Instruments). Probes were FESP with a pyramidal shape and end radius of 5−10 nm supplied by Digital Instruments and were utilized in the taping mode. Samples were attached to a 15-mm magnetic specimen disk with black carbon double-sided tape. Images were taken at scan sizes of 10 μm, 1 μm, and 200 nm. The scan angle was changed occasionally from 0° to 45° to check the integrity of the images.

Surface area, pore volume, and pore size distribution were measured by nitrogen adsorption−desorption using a Coulter SA 3100 (Miami, FL). The resulting isotherms were used to calculate the surface areas of the samples based on BET theory[18] and the pore volume and pore size distributions based on BJH (Barret, Joyner, and Hallenda) pore theory.[19]

Particle size analyses were obtained on a laser granulometer Malvern Mastersizer S using light scattering.

ATR-FTIR (attenuated total reflectance-FTIR) spectra of the **Lep** and **Goet**−**Lep** samples before and after AA adsorption were recorded on a Bruker Equinoxe 55 infrared spectrometer (Bruker, Gmbh, Karlsruhe, Germany). Spectra resolution was 2 cm^{-1}.

The atomic environment of iron within the ferroxane was determined using Fe K-edge X-ray absorption spectroscopy (XAS) on the dehydrated samples. The structural site of Zr of the doped ferroxane was characterized at the Zr K-edge. XAS consists of recording the absorption coefficient μ of a given sample as a function of the wavelength in the X-ray range. XAS spectra were recorded at room temperature in the transmission mode at the NSLS synchrotron (Brookhaven National Laboratory, Upton, NY) on the X23A2 EXAFS beamline. The positron storage ring was running at 1.85 GeV and 320 mA. EXAFS (extended X-ray absorption fine structure) data reduction was accomplished according to a procedure described previously.[12,20] The Fourier transform yields radial distribution functions (RDF) consisting of n peaks representing n coordination spheres at R_n distances from the central atom. Distances are uncorrected for phase shift and have to be displaced toward long distances by 0.3−0.4 Å from crystallographic positions. The structural and chemical parameters R_j, N_j (number of atoms j at R_j Å from Fe) and nature of atomic neighbors in the jth shell around Fe were determined by least-squares fitting of partial EXAFS spectra.[21] The uncertainties on R and N are 0.06 Å and 10%, respectively. EXAFS provides average structural information. If several Fe structural sites coexist within the sample, only the mean number of neighbors can be determined.

3. Results and Discussion

3.1. Structure of the Starting Material. As previously detailed, two products were used as the starting

(8) Kareiva, A.; Harlan, C. J.; MacQuenn, D. B.; Cook, R. L.; Barron, A. R. *Chem. Mater.* **1996**, *8*, 2331.
(9) Pourbaix, M. *Atlas d'Équilibres Électrochimiques*; Gauthier-Villars: Paris, 1963.
(10) Karthikeyan, K. G.; Elliott, H.A.; Chorover, J. *J. Colloid Interface Sci.* **1999**, *209*, 7278.
(11) Hingston, F. J.; Posner, A. M.; Quirk, J. P. *J. Soil Sci.* **1972**, *23* (2), 177.
(12) Rose, J.; Manceau, A.; Bottero, J. Y.; Masion, A.; Garcia, F. *Langmuir* **1996**, *12* (26), 6701.
(13) Rose, J.; Manceau, A.; Masion, A.; Bottero, J.-Y. *Langmuir* **1997**, *13*, 3240.
(14) Rose, J.; Vilgé, A.; Olivie-Lauquet, G.; Masion, A.; Frechou, C.; Bottero, J.-Y. *Colloids Surf. A* **1998**, *136*, 11.
(15) Doelsch, E.; Rose, J.; Masion, A.; Bottero, J.-Y.; Nahon, D.; Bertsch, P. *Langmuir* **2000**, *16*, 4726.
(16) Bayler, D. Master of Science, Rice University, 1999.
(17) Refait, P.; Génin, J.-M. R. *Corrosion Sci.* **1993**, *34* (5), 797.
(18) Brunauer, S.; Emmett, P. H.; Teller, E. *J. Am. Chem. Soc.* **1938**, *60* (11), 309.
(19) Barret, E. P.; Joyner, L. G.; Halenda, P. P. *J. Am. Chem. Soc.* **1938**, *123* (2), 165.
(20) Manceau, A.; Calas, G. *Clays Miner.* **1986**, *21*, 341.
(21) Teo, B. K.; EXAFS: Basic Principles and Data Analysis. *Inorganic Chemistry Concepts*; Springer-Verlag: Berlin, 1986.

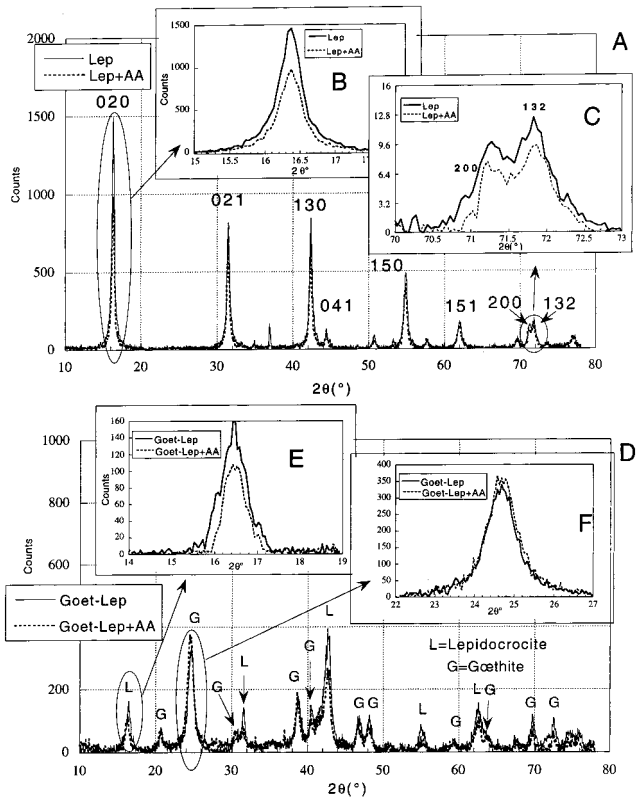

Figure 1. X-ray diagrams of the **Lep** and the **Goet**−**Lep** samples before and after the reaction with AA.

material to react with acetic acid. Minerals yielded from synthesis A were identified by XRD (Figure 1D) as a mixture of α- and γ-FeOOH (=**Goet**−**Lep** sample). In contrast, synthesis B led to 100% of pure lepidocrocite γ-FeOOH (=**Lep** sample) as can be seen on the diffractogram (Figure 1A). It is interesting to observe that the **Goet**−**Lep** is less crystalline than the **Lep** sample: the intensities multiplied by the fwhm (full-weight at half-maximum) of the peak at 16.45° corresponding to the 020 crystallographic plane of the lepidocrocite are different: 255 and 59 for the **Lep** and for the **Goet**−**Lep** samples, respectively. The decrease of the intensity of the peaks suggests that the ordered domain is smaller for the **Goet**−**Lep** than for the **Lep** sample. The fact that the fwhm of the peak is higher (0.32 vs 0.25) indicates that the product **Goet**−**Lep** is more disordered, that is, the interatomic distances are more distributed.

3.2. FeOOH + Acetic Acid → Ferroxane−**AA.** The reaction between FeOOH minerals and acetic acid (AA) produced red products. The analysis of the total organic carbon (TOC) in the supernatant indicated that ≈15% of AA was sorbed to the **Goet**−**Lep** and **Lep** samples. This result suggests that an average of 0.225 Fe atoms are linked to 1 AA. The concentration of Fe in the supernatant indicates that only 0.2% of the Fe is dissolved from both starting materials.

The analysis of the size distribution of the **Lep** sample and the resulting **ferroxane**−**AA** indicates that the size of the particles of the initial mineral decreases from 30 to 0.3 μm (Figure 2). The particles resulting from the process present a relatively monodisperse size distribution around 0.3 μm. The size decrease from the parent material might be attributed to either a dissolution or

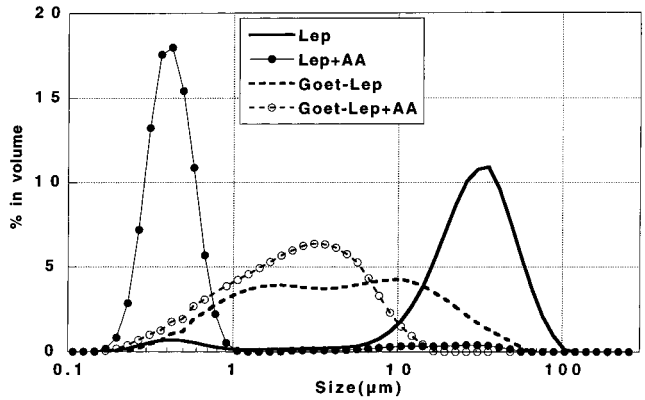

Figure 2. Particles size distributions of the parrent material and resulting ferroxanes as determined by light scattering.

a cleavage−breakage of the particles. The low concentration of Fe in the supernatant suggests that dissolution is not the driving force for the size decrease. Cleavage or breakage of the γ-FeOOH mineral is similar to the formation of alumoxane from the γ-AlOOH mineral. Callender et al.[5] indicated that the size of the C−alumoxane resulting from the reaction between γ-AlOOH particles (50−100 μm in size) and AA was ≈50 nm. A comparison between cleavage and breakage of the particles is discussed below.

Acetic acid reacted with the **Goet**−**Lep** sample produced a different product. The size of the initial **Goet**−**Lep** particles was between 1 and 10 μm but the size of the resulting product after reacting with AA was larger and more broadly distributed than in the case of the **Lep** sample (Figure 2). Thus, it seems that AA has some impact on the decrease of the size of the particles. Knowing that the **Goet**−**Lep** sample is composed of lepidocrocite and goethite particles and that the size of the lepidocrocite particles is strongly affected by AA (as shown previously), we can reasonably conclude that the size of the goethite particles is not reduced greatly after reaction with AA. The analysis of the X-ray diffractograms (Figure 1) confirms this hypothesis: α-FeOOH is less affected by the AA than the γ-FeOOH. In the case of the **Lep** sample, composed only of γ-FeOOH, the intensity of the diffraction peaks decreased when **Lep** reacted with AA (Figure 1a). The fwhm multiplied by the intensity of the peak corresponding to the 020 atomic plane decreased from 555 to 378 AU (Figure 1b). This evolution corresponds to a decrease in the size of the ordered domain. In the case of the **Goet**−**Lep** sample, composed of α- and γ-FeOOH, the diffraction peaks of the lepidocrocite mineral decreases (fwhm**I* of the peak 020 of the lepidocrocite decreases from 93.0 to 58.8, Figure 1e) while the intensity of the peaks corresponding to α-FeOOH are not modified (*I**fwhm of the peak 101 of the goethite = 297−315, Figure 1f). In this case, α-FeOOH is not modified by AA. Thus, the structure of the initial FeOOH mineral is the key factor in producing ferroxane.

By examining the decrease of the intensity of the different diffraction peaks of the lepidocrocite mineral from the **Lep** material, we can conclude that the AA cleaves and breaks the lepidocrocite. Both mechanisms appear during the formation of ferroxane. The fwhm**I* value for the peak of the 020 crystallographic plane decreased by 32%. Because along the *b* axis the layer

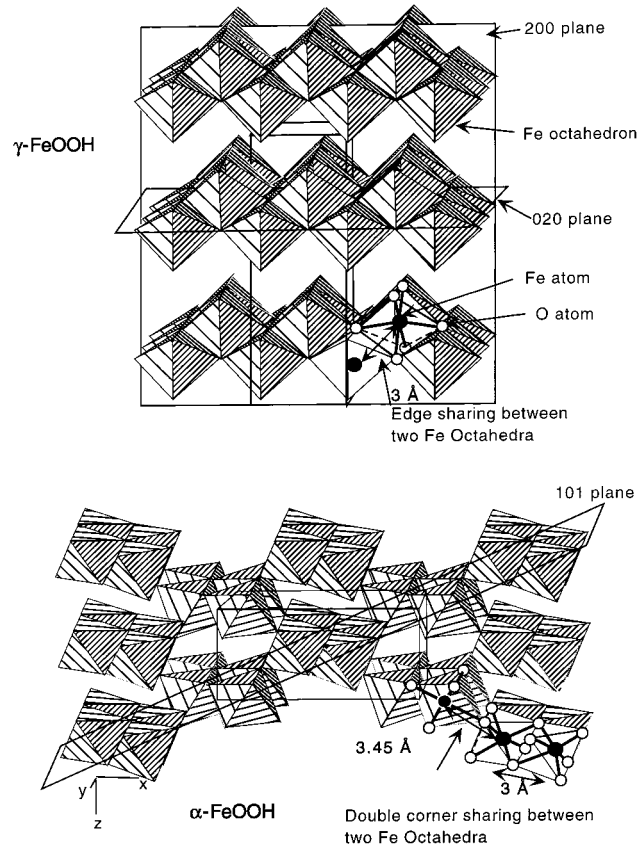

Figure 3. Struture of the γ- and α-FeOOH.

constituted by Fe octahedra planes are separated by hydrogen bonds (Figure 3), it seems that AA cleaves the Fe Layers. The peak corresponding to the 200 plane decreased by 40%. Thus, the fact that the coherent domain also decreased in the $a-c$ direction suggests that the Fe layers are broken (Figure 3).

Therefore, it seems that AA has two effects on γ-FeOOH: it cleaves and breaks the mineral while the α-FeOOH is not affected. The fact that γ-FeOOH is cleaved and α-FeOOH is not can be linked directly to their 3D structure. γ-FeOOH consists of layers made of Fe octahedra. Each Fe octahedron is linked to six other Fe through edge sharing (Figure 3). All planes are linked with other through hydrogen bonding. In the case of α-FeOOH each Fe octahedron is linked to four other Fe octahedra through edge sharing and four others through double corner sharing (Figure 3). Then, it appears that the 3D structure of α-FeOOH is reinforced by chemical linkages while in the case of γ-FeOOH the cohesion is due to weaker hydrogen bonds that can be cleaved by AA. Once the mineral is cleaved, the Fe layers are less resistant and can be broken. No great differences in dissolution of these minerals were observed, suggesting that the energy of Fe−O−Fe and Fe−OH−Fe bonds are similar for both minerals.

To further describe the structural evolution of **Goet−Lep** and **Lep** materials reacting with AA, EXAFS experiments were performed at the Fe K edge. The results of the modeling curves (Table 1) indicate that the number of Fe atoms around each Fe (=N_{Fe} = mean value) decreases from 6 ± 10% to 4.5 ± 10% for the **Lep** and **Lep + AA** sample, respectively. This decrease can be attributed to two phenomena. The first one is a

Table 1. Structural Parameters Derived from EXAFS Analysis at the Fe K Edge of the Lep + AA and Goet−Lep + AA Samples

compound	shell	R (Å)	N	σ (Å)	Q^a
Lep	Fe	3.06	6.0	0.080	0.002
Lep + AA	Fe	3.06	4.5	0.084	0.050
Goet−Lep	Fe	3.07	3.5	0.072	0.080
	Fe	3.38	2.4	0.081	
Goet−Lep + AA	Fe	2.95	2.0	0.075	0.016
	Fe	3.38	3.2	0.085	
	C	3.08	1.3	0.030	

[a] $Q = \sum[(k^3\chi_{calculated} - k^3\chi_{experimental})]^2/(k^3\chi_{experimental})^2$.

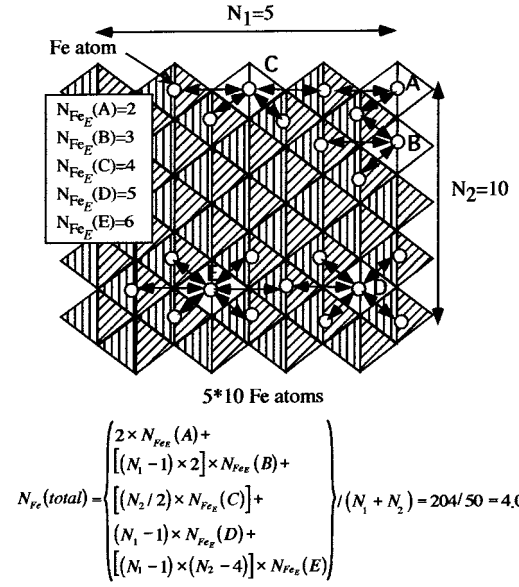

Figure 4. Structure of a γ-FeOOH Fe layer and calculation of the average number of Fe neighbors.

decrease in the size of the ordered domain and the second one is the creation of vacant crystallographic sites. XRD results favor the first hypothesis.

With N_{Fe} we can try to estimate the size of the ordered domain. In the case of an "infinite" lepidocrocite particle each Fe atom is surrounded by six other Fe at a distance of 3 Å.[22] This distance of 3 Å between two Fe atoms corresponds to edge linkage between two Fe octahedra (Figure 3). The number of these edge linkages between Fe octahedra is called N_{Fe_E}. If the size of each Fe layer decreases, the proportion of border Fe atoms surrounded by less than six Fe atoms increases. Thus, the average N_{Fe} becomes lower than 6. Figure 4 presents an Fe layer with the lepidocrocite structure and details the theoretical N_{Fe} value for this layer. If the layer is composed of 5 × 10 ($N_1 = 5$ and $N_2 = 10$) Fe octahedra, the average N_{Fe} will be

$$N_{Fe} = 4.08 = [2 \times N_{Fe_E}(A) + [(N_1 - 1) \times 2] \times N_{Fe_E}(B) + [(N_2/2) - 2] \times N_{Fe_E}(C) + (N_1 - 1) \times N_{Fe_E}(D) + [(N_1 - 1) \times (N_2 - 4)] \times N_{Fe_E}(E)]/(N_1 \times N_2) = 204/50$$

with $N_{Fe_E}(A) = 2$, $N_{Fe_E}(B) = 3$, $N_{Fe_E}(C) = 4$, $N_{Fe_E}(D) = 5$, $N_{Fe_E}(E) = 6$. A, B, C, D, and E indicate the different Fe sites shown in Figure 4.

(22) Christensen, H.; Christensen, A. N. *Acta Chem. Scand.* **1986**, *A32*, 87.

For the sample **Lep + AA = ferroxane−AA**, $N_{Fe} = 4.5 \pm 10\%$. Let us try to define the size of an Fe layer for $N_{Fe} = 4$ and 5. For an Fe layer composed of 5×10 ($=N_1 \times N_2$) Fe atoms, $N = 4.08$ and for a 10×20 Fe layer, $N_{Fe} = 4.995$. For these two layers the size is approximately 21×15 and 40×31 Å^2, respectively. This result underscores the variation of the size of the Fe layer versus a low variation of the N_{Fe} value. Given an accuracy of ±10% on N_{Fe}, it is difficult to determine the size of the ordered domain. Nonetheless, for a N_{Fe} value of 5 ± 0.5 the diameter of the layer would be in the ≈15−35 Å range. In a first approximation we can assign an average diameter of the ordered domain of 25 (±10) Å. This size of the ordered domain does not correspond necessarily to the size of the ferroxane particles since a particle can be a juxtaposition of ordered nanodomains. In our case it seems that the particles of 0.3 μm are constituted by nanodomains of 20−30 Å.

For the initial **Goet−Lep** sample each Fe is surrounded by 3.5 Fe at a distance of 3 Å (edge linkage between Fe octahedra $= N_{Fe_E}$) and 2.4 Fe at a distance of 3.4 Å (double corner sharing $= N_{Fe_{DC}}$). As observed before, XRD results indicate the presence of goethite and lepidocrocite for this initial product. In the case of a sample composed of pure and well-crystallized α-FeOOH, $N_{Fe_E} = 4$ and $N_{Fe_{DC}} = 4$.[23] If the ordered domains are not infinite, N_{Fe_E} and $N_{Fe_{DC}}$ will be lower than 4 but $N_{Fe_E} = N_{Fe_{DC}}$. In our case $N_{Fe_{DC}} = 2.4$. If the sample is composed of 100% of α-FeOOH, N_{Fe_E} would be equal to $2.4 = N_{Fe_{DC}}$. But $N_{Fe_E} = 3.6$ suggests that the sample is also composed of γ-FeOOH. For a sample with 100% goethite $N_{FeE} = 2.4$, then (2.4/3.6 = 0.66) 66% of the product is estimated to be α-FeOOH. This proportion is an approximation since the size of the microdomains and the presence of amorphous FeOOH are not taken into account for this calculation. After reaction with AA, N_{Fe_E} decreases while $N_{Fe_{DC}}$ increases. This result suggests that either the proportion of α-FeOOH increases versus γ-FeOOH or that the microdomains of the lepidocrocite decrease and the α-FeOOH domains are not affected. This result is in agreement with previous results, indicating that the lepidocrocite is cleaved and broken while α-FeOOH is not affected by AA.

The last point to discuss concerns the AA interaction with both minerals. ATR-FTIR spectra of the **Lep**, **Lep + AA**, **Goet−Lep**, and **Goet−Lep + AA** samples have been recorded to better identify the adsorption mechanism of AA at the mineral surface. The FTIR spectra of the four samples in the most interesting range (950−1850 cm^{-1}) are shown in Figure 5. The spectra of the **Lep** and the **Goet−Lep** samples are extremely similar in the domain of interest. The spectra of the two samples after reaction with AA, **Lep + AA** and **Goet−Lep + AA**, present new bands at 1260, 1421, and 1585 cm^{-1} and a shoulder at 1714−1720 cm^{-1} compared to the FTIR of the **Lep** and **Goet−Lep** curves. Absorption bands in the 1300−1200 cm^{-1} area are characteristic of C−O stretching.[24,25] This band is present on the

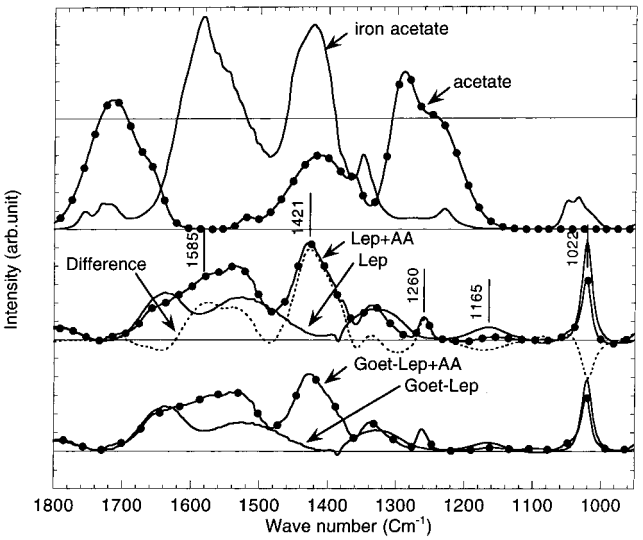

Figure 5. ATR-FTIR spectra in the region 1800−950 cm^{-1}.

spectrum of the acetate at 1294 cm^{-1} and is noticeably shifted on the **Lep + AA** and **Goet−Lep + AA** FTIR curves (1260 cm^{-1}). This shift can be due to the adsorption of the carboxylate group of the acetate at the lepidocrocite and goethite surfaces. This shift has also been observed by Gu et al.[24] and was interpreted as the complexation between the C−O functional group and iron oxide surface. The band present at 1421 cm^{-1} can be assigned to COO vibration[24]) and confirms the C−O complexation to Fe. In the case of interaction between soil fulvic acid and Fe that forms iron fulvate, this band exists.[24] This band is also present on the FTIR curve of the iron acetate compound for which the acetate is complexed to Fe through a monodentate linkage type: Fe−O−C. The band presents at 1585 cm^{-1} on the **Lep + AA**, **Goet−Lep + AA** and the iron acetate FTIR curves correspond to C−O vibrations of carboxylate groups.[25,26] In the case of the acetate compound for which the carboxylate group is not complexed to Fe, this band is shifted at 1714 cm^{-1} with a shoulder at 1690 cm^{-1}.[27] This important shift is additional evidence for the carboxylate complexation with the FeOOH surface. The great similarities between the IR bands of the iron acetate and the **Lep + AA** and **Goet−Lep + AA** FTIR curves lead to the conclusion that AA is adsorbed through the monodentate complex at the lepidocrocite and goethite surface. These adsorption complexes have also been evidenced with Fe K edge EXAFS. A Fe−C contribution at 3.08 Å is detected for the **Goet−Lep + AA**. This is due to the presence of Fe−O−C linkages. This distance could correspond to a monodentate complex. For this kind of linkage the Fe−C distance varies between 3.0 and ≈3.4 Å depending on the Fe−O and C−O distances and Fe−O−C angles. This is the case for several reference compounds analyzed from the CSD database (more than 230.000 organic and organometallic compounds) ($C_{58}H_{74}FeN_6O_{12}\cdot 2(C_2H_6O)$ → Fe−C = 3.4 Å,[28] $C_{18}H_{22}FeN_2O_9)_n\cdot 2n(H_2O)$ → Fe−C = 3.0 Å, [29]

(23) Szytula, A.; Burewicz, A.; Dimitrijevic, Z.; Krasnicki, S.; Rzany, H.; Todorovic, J.; Wanic, A.; Wolski, W. *Phys. Status Solidi* **1968**, *26*, 429.
(24) Gu, B.; Schmitt, J.; Chen, Z.; Liang, L.; McCarthy, J. F. *Environ. Sci. Technol.* **1994**, *28*, 38.
(25) Bruker Infra-red Tables, 2001, p 50, www.bruker.com.
(26) Gupta, S. K.; Kushwah, Y. S. *Polyhedron* **1994**, *20*, 2019.
(27) Bacchi, A.; Ivanovic-Burmazovic, I.; Pelizzi, G.; Andjelkovic, K. *Inorg. Chim. Acta* **1994**, *313*, 109.
(28) Baker, E.; Maslen, E. N.; Watson, K. J.; White, A. W. *J. Am. Chem. Soc.* **1984**, *106*, 2860.
(29) Jameson, D. L.; Chuang-Liang, X.; Hendrickson, D. N.; Potenza, J. A.; Schugar, H. J. *J. Am. Ceram. Soc.* **1987**, *109*, 740.

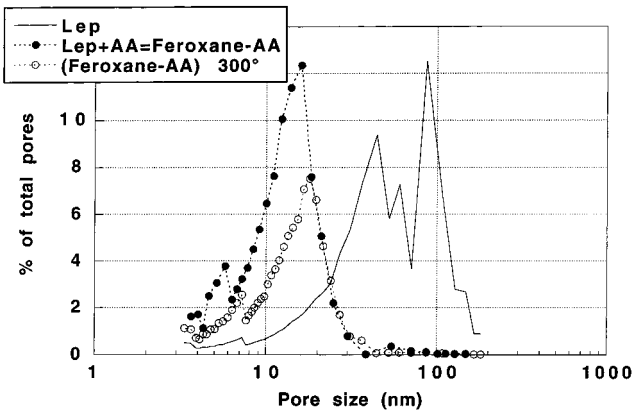

Figure 6. Adsorption pore volume distribution.

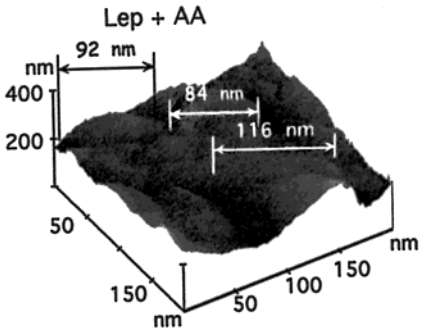

Figure 7. 200 nm AFM image of the **ferroxane−AA** sample.

$C_{32}H_{38}FeO_{22}$ → Fe−C = 3.2 Å,[30] etc.). Even if the Fe−C distance for a monodentate complex can vary in a large range, especially due to the variation of the Fe−O−C interatomic angle, in the case of a bidentate complex, the Fe−O−C distance is generally lower than 3.01 Å. For binuclear bidentate complexes the Fe−C distance is in the 2.40−3.01 Å range. This is the case for the different compounds analyzed from the CSD database: $C_{24}H_{26}Fe_4N_4O_{26}\cdot 6(Na)\cdot 20(H_2O)$ (Fe−C = 3.00 Å[31]), $Fe_2N_2O_{16}K_4\cdot 2(CH_4O)\cdot 2(H_2O)$ (Fe−C = 2.91 Å[32]), $C_{29}H_{36}Fe_2N_8O_4I_2\cdot 6(H_2O)$ (Fe−C = 3.01 Å[33]), $C_{20}H_{42}Fe_2N_6O_7\cdot 4.25(H_2O)$ (Fe−C = 2.97 Å[34]), $C_{60}H_{120}Fe_6N_{12}O_{24}$ (Fe−C = 2.95 and 3.01 Å[35]), $C_{11}H_4FeN_2O_9\cdot 5(H_2O)$ (Fe−C = 2.47 Å[36]), $C_{39}H_{76}Fe_3N_3O_{14}\cdot C_7H_8$ (Fe−C = 2.96 Å[37]). No bidentate complex was found from the CSD database with an Fe−C distance higher than 3.01 Å. The fact that the Fe−C distances of bidentate complexes are lower than 3.01 Å is due to lower Fe−O−C angle values. For these types of structures the Fe−O−C interatomic angle never exceeds 133°. One can criticize our conclusion since the distance determined with EXAFS is 3.08 Å and is not so different from the Fe−C distance for bidentate

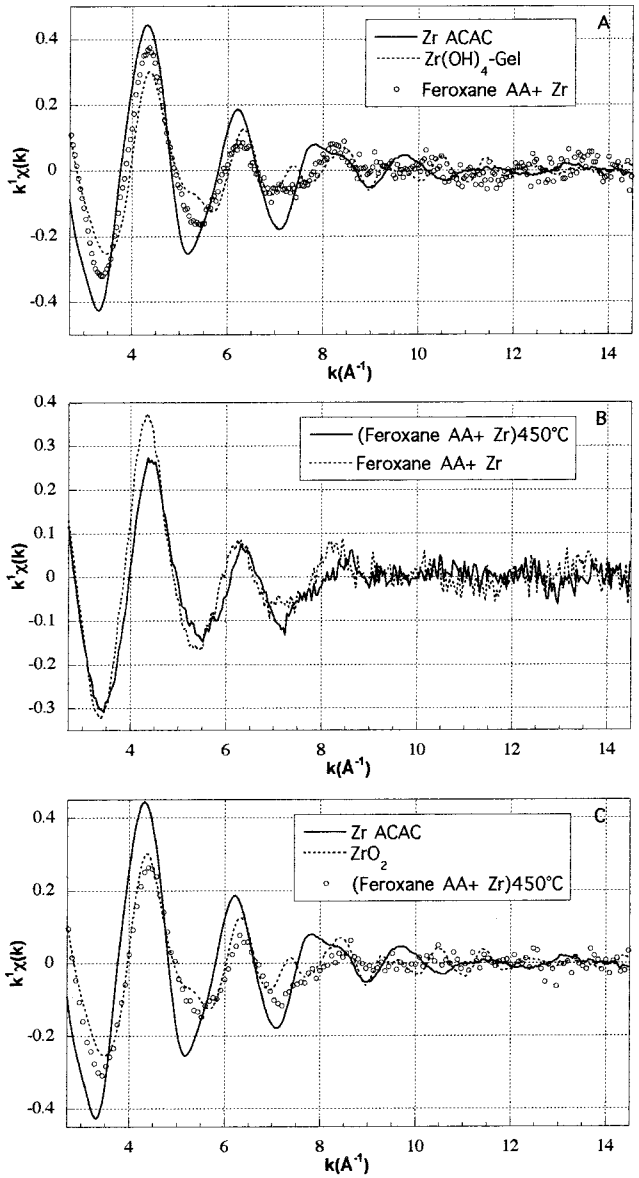

Figure 8. EXAFS spectra for the **ferroxane−AA + Zr** and the **(ferroxane−AA + Zr)450°C** samples and several refence compounds.

complexes. In the case of EXAS analysis the uncertainty on the number of neighbors can be high and never lower than 10%, but the interatomic distances are generally determined with great accuracy: ±0.01−0.03 Å. Thus, our hypothesis concerning the type of linkage seems reasonable.

All these results suggest that AA is chemically adsorbed at the FeOOH surface through a monodentate complex and is in marked contrast with results reported for alumoxane for which a bidentate complex was identified.[5] The lack of an apparent Fe−C contribution detected by Fe K edge EXAFS in the case of the **Lep + AA** sample does not necessarily mean that this contribution is absent. XRD measurements revealed that the **Goet−Lep** is less crystallized than the **Lep** sample. Thus, the number of surface Fe's is certainly higher in the **Goet−Lep** sample than in the **Lep** sample, leading to a higher proportion of Fe−O−C linkages for the **Goet−Lep** sample.

In summary, it appears that AA cleaves and breaks only the lepidocrocite, yielding new products. In the case

(30) Morelock, M. M.; Good, M. L.; Trefonas, L. M.; Majeste, R.; Karraker, D. G. *Inorg. Chem.* **1982**, *21*, 3044.
(31) Bruce, M. I.; Walton, J. K.; Williams, M. L.; Patrick, J. M.; Skelton, B. W.; White, A. H. *J. Chem. Soc., Dalton Trans.* **1983**, 815.
(32) Fujita, T.; Ohba, S.; Nishida, Y.; Goto, A.; Tokii, T. *Acta Crystallogr., Sect. C* **1994**, *50*, 544.
(33) Arulsamy, N.; Hodgson, D. J.; Glerup, J. *Inorg. Chim. Acta* **1993**, *209*, 61.
(34) Drueke, S.; Wieghard, K.; Uber, B. N.; Weiss, J. *Inorg. Chem.* **1989**, *28*, 1414.
(35) Dell'Amico, D. B.; Calderazzo, F.; Labella, L.: Maiche-Mossmer, C.; Strahle, J. *Chem. Commun.* **1994**, 1555.
(36) Ruiz, R.; Triannidis, M.; Aukauloo, A.; Journaux, Y.; Fernandez, I.; Pedro, J. R.; Cervera, B.; Castro, I.; Munoz, M. C. *Chem. Commun.* **1997**, *22*, 83.
(37) Hummel, H.; Bill, E.; Weyhermuller, T.; Wieghardt, K. *Inorg. Chim. Acta* **1997**, *291*, 258.

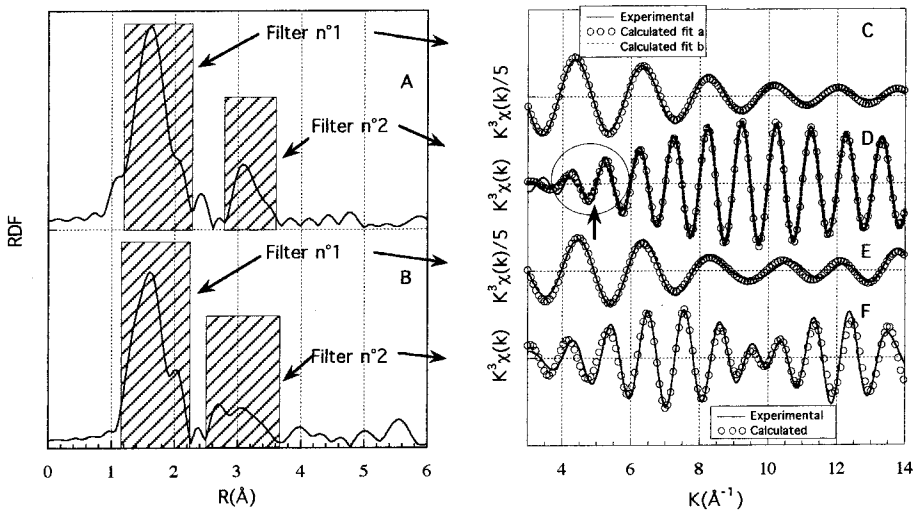

Figure 9. Radial distribution functions (RDF) for the **ferroxane−AA + Zr** (A) and **(ferroxane−AA + Zr)450°C** (B) samples. Dashed areas correspond to the filters used for the back-Fourier transforms. Experimental and calculated partial EXAFS spectra corresponding to the back-Fourier transforms of each filter (C) for **ferroxane−AA + Zr** (filter 1), (D) **ferroxane−AA + Zr** (filter 2), (E) for **(ferroxane−AA + Zr)450°C** (filter 1), (F) for **(ferroxane−AA + Zr)450°C** (filter 2).

of the **Lep** material, particles ≈0.3 μm in size are formed with a core structure of γ-FeOOH and an AA external coat. We call this new product **ferroxane−AA**.

3.3. Texture of the Ferroxane−AA. The specific surface area measured by nitrogen adsorption does not evolve after the reaction of lepidocrocite with AA, remaining more or less constant at values of 137−134 m^2/g. In contrast, the distribution of pores within the pore size **Lep** and ferroxane samples differed considerably (Figure 6). The average pore size diameter decreases from 53 nm for the **Lep** sample to 12 for the **ferroxane−AA**. Moreover, the fwhm of the pore size distribution for the **ferroxane−AA** is weaker than that for the **Lep** sample and the distribution is narrower.

The texture of the surface of **ferroxane−AA** was investigated with AFM. A diameter of 100 nm was estimated for the ferroxane particles (Figure 7). Given the differences in methods used in each case, this value is in reasonable agreement with the diameter determined by light scattering (300 nm).

3.4. From Ferroxane to Ceramic. Ferroxane−AA particles produced from a Lepidocrocite/AA reaction were deposited on a substrate and fired at 300 °C. The resulting product was identified by XRD as hematite. The specific area increases from 134 for the **ferroxane−AA** to 144 m^2/g for the α-Fe_2O_3 while the average pore size remained constant at 12.7−13.5 nm (Figure 6).

3.5. Doped Ferroxane. The reaction between ferroxane and zirconium acetylacetone (=Zracac) was chosen for the purposes of comparing the doped ferroxane with doped alumoxane reported by Kareiva et al.[8] The reaction between alumoxane and M(acac) proceeds as follow: $[Al(O)_x(OH)_y(O_2(R)_z] + yM(acac)_3 \rightarrow [Al(O)_x\text{-}\{OM(acac)_n\}_y(O_2(R)_z] + y(acac-H)$. We evaluated the possibility of an analogous reaction with ferroxane.

The first point to know concerning the doping mechanism is to determine whether Zracac reacts with the **ferroxane−AA**. The second point is to know whether the Zr site evolves during the firing or not. The XAS spectroscopy at the Zr K edge has been used since this technique provides information at the atomic scale on the nature, number, and distance of the atomic neighbors of Zr.

Table 2. Structural Parameters Derived from EXAFS Analysis at the Zr K Edge of the Ferroxane−AA + Zr and (Ferroxane−AA + Zr)450°C Samples

compound	fit	shell	R (Å)	N	σ (Å)	Q^a
ferroxane−AA + Zr	fit a	Fe	3.34	0.4	0.02	0.012
		Fe	3.62	4.8	0.100	
	fit b	Zr	3.48	0.4	0.02	0.016
		Fe	3.66	2.2	0.080	
(ferroxane−AA + Zr)450°C		Fe	3.08	1.2	0.060	0.006
		Zr	3.42	4.6	0.110	

[a] $Q = \Sigma[(k^3\chi_{calculated} - k^3\chi_{experimental})]^2/(k^3\chi_{experimental})^2$.

Figure 8a presents the EXAFS curves of Zracac, Zr-$(OH)_4$ gel, and **ferroxane−AA + Zr**. The fact that the curves of Zracac and **ferroxane−AA + Zr** are different suggests that the atomic environment of Zr has changed during the reaction between **ferroxane−AA** and the Zracac solution. The normal effect of Zracac in water, when the pH is ≈4−5, is to polymerize and to form zirconia gels.[38] Differences between the EXAFS curves of the zirconia gel and the **ferroxane−AA + Zr** lead to the conclusion that the Zracac has reacted with the particles of **ferroxane−AA**.

Modeling of the partial EXAFS curves corresponding to the back-Fourier transforms of the two peaks of the RDF in the 1.2−2.2 and 2.6−3.6 Å range were done using Zr−O, Zr−Zr, and Zr−Fe contributions (Table 2, Figure 9). The first-coordination sphere of Zr in the **ferroxane−AA + Zr** sample is composed of 6 (±10%) oxygen atoms at 2.10 and 2.28 Å. This result shows that the zirconium is in a new atomic environment since the first-coordination sphere of Zr in Zracac is constituted of 8 oxygen atoms at 2.2 Å (in average).[39] The partial EXAFS curve corresponding to the second-coordination sphere was fit using Fe and Zr contributions. These two calculations (fit a and b Table 2, Figure 9d) lead to good adjustments of the experimental curve (Figure 9d). Only a slight difference can be observed in the low K region, suggesting that the calculation using two Fe shells

(38) Peter, D.; Ertel, T. S.; Bertagnolli, H. *J. Sol−Gel Sci. Technol.* **1995**, *5*, 5.
(39) Silverton, J. V.; Hoard, J. L. *Inorg. Chem.* **1963**, *2*, 243.

instead of one Fe and one Zr shell around Zr gives a better adjustment. Thus, Zr is surrounded by 5 Fe; that is, Zr is incorporated within the structure of the **ferroxane−AA** and is not only adsorbed. The Zr−Fe interatomic distances of 3.3 and 3.6 Å are in the same range as distances found for other Fe−Zr oxides (3.3 Å for the $Fe_xZr(Ti)_{1-0.75x}O_{2-\delta}$;[40] 3.4 and 3.7 Å for the hiortdahlite;[41] 3.48 Å for the janhaugite[42]).

After firing, the Zr environment changes (Figure 8b,c) and Zr does not evolve to form ZrO_2 particles as evidenced by the fact that the EXAFS curves of **ferroxane−AA + 450 °C** and ZrO_2 are different. Modeling of the partial EXAFS curves indicates that the first-coordination sphere has not significantly changed from **ferroxane−AA + Zr** (Table 2). Concerning the second-coordination sphere, it appears that Zr is still incorporated in the Fe_2O_3 mineral (a Zr−Fe contribution is detected) but that the presence of Zr in that sphere indicates that the site evolved and that some Zr−O−Zr clusters exist.

4. Conclusion

We have demonstrated that the reaction between lepidocrocite and acetic acid (=AA) in water results in the formation of carboxylate−FeOOH nanoparticles called ferroxane−AA. The structure of ferroxane consists of an FeOOH core part with the structure of the lepidocrocite, coated with AA. EXAFS at the Fe K edge indicates that AA is chemically adsorbed onto an FeOOH core. The size of these ferroxanes is 0.3 μm and is composed of nanodomains of 0.02 μm with a γ-FeOOH structure. Thermolysis of the ferroxane−AA yields Fe−ceramic with the crystallographic structure of hematite. The specific surface area ($\approx$134 m^2/g) does not increase from the initial FeOOH mineral to the ferroxane−AA and the Fe−ceramic, while the pore size distribution becomes more monodisperse and the diameter of the pore size decreases from 55 to 12 and 13 nm after firing of the ferroxanes.

The ferroxane−AA was successfully doped with zirconium. The Zr is incorporated within the structure of the ferroxane−AA. After firing of these samples, a mixed Fe−Zr oxide is formed.

Acknowledgment. The authors thank the INSU for supporting this research through the ATI no. 99. They also thank J. Woicik and Z. Fu in charge of the X23A2 beamline of the National Synchrotron Light Source (Brookhaven National Laboratory, Upton, NY) for their helpful and kind assistance. Research carried out (in part) at the NSLS was supported by the U.S. Department of Energy, Division of Materials Sciences and Division of Chemical Sciences under Contract no. DE-AC02-98CH10886. Work was also partially supported under the National Science Foundation Center for Biological and Environmental Nanotechnology at Rice University.

CM010583R

(40) Tsodikov, L. V.; Bukhtenko, O. V.; Ellert, O. G.; Shcherbakov, V. M.; Kochibey, D. I. *J. Mater. Sci.* **1995**, *30*, 1087.
(41) Merlino, S.; Perchiazzi, N. *Tschermaks Mineral. Petrogr. Mitt.* **1985**, *34*, 297.
(42) Annehed, H.; Faelth, L.; Raade, G. *J. Neues Jahrbuch Mineral. Abhandlungen* **1985**, 7.